Analysis and Simulation of AC-Biased TES Circuits

Tian-Shun Wang, Jun-Kang Chen, and Xingxiang Zhou

***Abstract*—We systematically study the analysis and simulation of ac-biased superconductor transition-edge sensor (TES) circuits. In these ac-biased circuits, the current and voltage of the TES experience large swings in both directions, and small-signal analysis around a dc steady state does not apply. To understand their electrical and thermal behavior, we rely on concepts and techniques from radio-frequency circuit simulation and introduce the periodic steady state and perform periodic ac analysis. We also construct TES device models based on a comprehensive two-fluid physical model and investigate the behavior of ac-biased TES circuits using advanced circuit simulators. By relating our findings to results for the analysis of dc-biased TES circuits, we give appropriate definitions for the current and temperature sensitivity of the TES in ac-biased circuits. Our work not only builds a rigorous foundation for theoretical analysis of ac-biased TES circuits but also introduces powerful simulation techniques valuable for their design and research.**

***Index Terms*—Circuit analysis, computer simulation, superconducting devices.**

I. Introduction

SUPERCONDUCTOR transition-edge sensors (TESs) have played a critical role in many scientific projects and instrumental applications. As one noteworthy example, detection of B-mode polarization was performed [1] recently using bolometer arrays with hundreds of TESs. In future applications, it is expected that even larger-scale TES detectors will come into use.

Key to the realization of large-scale TES detectors is the development of multiplexing technology that allows for reading out the signals of multiple TESs with the same readout circuitry. Among the possible multiplexing techniques, frequency-domain multiplexing (FDM) is an attractive option being considered for important scientific missions such as SAFARI [2] and ATHENA [3]. At the core of FDM is the ac-biased TES circuit shown in Fig. 1. Considering the importance of ac-biased TES circuits to FDM, a rigorous framework for their analysis is needed. Unfortunately, the operational principles of ac-biased TES circuits are not well understood even in theory despite previous work [4], [5], and it remains an open question how their performance limit compares with that of dc-biased circuits. The main difficulty lies in the fact that, unlike in a dc-biased circuit as shown in Fig. 2, the TES current and voltage experience large swings in both directions in an ac-biased circuit (see Fig. 4). Consequently, all electrical and thermal quantities are changing at all times even in the absence of an input signal. In particular, the effective resistance of the TES can vary by a large amount in each cycle of the oscillation of the bias voltage (see Fig. 5). In such a situation, it

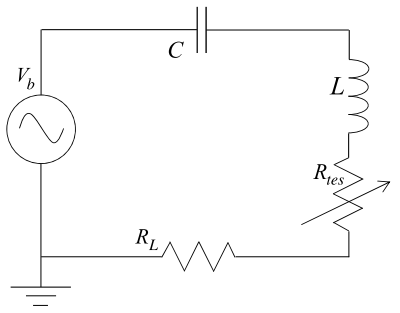

Fig. 1. AC-biased TES circuit. The frequency of the bias voltage $\omega_0 = 1/\sqrt{LC}$, where L and C are the inductance and capacitance in the circuit. Like in our earlier work [10], [11], TES device parameters for circuit simulation are either taken directly from [18] or inferred from experimental data in it. Specifically, the critical temperature, 0-temperature critical current, heat capacity, and normal resistance of the TES are $T_c = 105$ mK, $I_{c0} = 35$ μA, $\gamma = 3.3$ fJ/K, and $R_n = 1.6$ Ω. The resistance $R_L = 17.5$ mΩ is the sum of the parasitic resistance and the internal resistance of the bias voltage. The heat conduction exponent and the coefficient are $n = 5$ and $K = 16.54\,\mathrm{nW/K}^5$. The parameter $C_R = 1$ in (16). The substrate temperature is set at $T_b = 55$ mK. L and C are chosen to be 50 nH and 100 μF, unless otherwise stated.

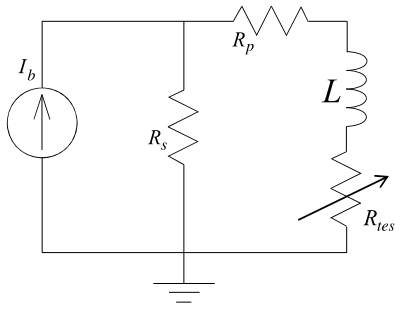

Fig. 2. DC-biased TES circuit. R_p is the parasitic resistance in the circuit. Since the shunt resistance R_s is much smaller than the TES resistance R_{tes}, the TES is effectively biased by a voltage source of $I_b R_s$ in series with an effective resistance $R_L = R_p + R_s$.

Manuscript received October 29, 2014; revised April 30, 2015 and July 28, 2015; accepted July 30, 2015. Date of publication September 3, 2015; date of current version September 12, 2015. This work was supported in part by the National Natural Science Foundation of China under Grant 11273023 and in part by the Central Government University Fundamental Research Fund. This paper was recommended by Associate Editor A. Kleinsasser.

T.-S. Wang was with the Department of Optics and Optical Engineering, the CAS Laboratory of Quantum Information, and the Synergetic Innovation Center of Quantum Information and Quantum Physics, University of Science and Technology of China, Hefei 230026, China. He is now with the Quantum Engineering Research Center, Beijing Institute of Aerospace Control Devices, China Aerospace Science and Technology Corporation (CASC), Beijing 100854, China.

J.-K. Chen and X. Zhou are with the Department of Optics and Optical Engineering, the CAS Laboratory of Quantum Information, and the Synergetic Innovation Center of Quantum Information and Quantum Physics, University of Science and Technology of China, Hefei 230026, China (e-mail: xizhou@ustc.edu.cn).

Color versions of one or more of the figures in this paper are available online at http://ieeexplore.ieee.org.

Digital Object Identifier 10.1109/TASC.2015.2470668

is no longer mathematically feasible to define time-independent temperature and current sensitivity, i.e.,

$$\alpha = \frac{T_{ss}}{R_{ss}} \frac{\partial R}{\partial T}\Big|_{I_{ss}} \tag{1}$$

$$\beta = \frac{I_{ss}}{R_{ss}} \frac{\partial R}{\partial I} z\Big|_{T_{ss}} \tag{2}$$

at dc steady-state values of current (I_{ss}), temperature (T_{ss}), and resistance (R_{ss}) and characterize the electrical property of the TES with an effective resistance obtained by Taylor expansion around R_{ss} as in small-signal analysis of dc-biased circuits.

To gain better understanding of ac-biased TES circuits and put their analysis on a mathematically rigorous ground, we use concepts and techniques from radio frequency (RF) circuit simulation to study their behavior. Not only is such work necessary for the development of FDM technology, but it is also important for the completeness of the theoretical framework of TES circuit analysis. From the results, we will be able to visualize how the electrical and thermal quantities impact each other in ac-biased circuits and understand how the temperature and current sensitivity should be defined. We also introduce simulation techniques unavailable in TES research before to predict the behavior of ac-biased TES circuits accurately. Such techniques can elevate the design of ac-biased TES circuits to a much more quantitative and reliable level and are thus a powerful tool for TES research.

II. Preliminary Work

The basics of the concepts and techniques we use for circuit analysis in this work were developed in the 1990s to meet the challenge of rapidly advancing wireless communication technology [6]. Since they are unfamiliar to the majority of the TES research community, a progressive approach is needed to make the treatment easier to understand. Here, we prepare for further in-depth study by introducing previously developed knowledge and tools that are useful in our analysis and presentation.

A. Review on Small-Signal Analysis of DC-Biased TES Circuits

As we emphasized in the introduction, small-signal analysis around a dc bias point is *NOT* applicable to ac-biased TES circuits. Nevertheless, when we discuss methods and techniques for the analysis and simulation of ac-biased TES circuits, it is very helpful to relate them to their conceptual counterparts in dc circuit analysis, which most researchers are familiar with. For this consideration, we give a brief review on small-signal analysis in the following.

Small-signal analysis of the dc-biased TES circuit in Fig. 2 starts with a steady state that can exist when the circuit parameters and bias conditions are appropriate. The electrical and thermal behavior of the dc-biased TES circuit is described by the following pair of equations [7]–[9]:

$$L\frac{dI}{dt} = I_b R_s - R_{tes}(I,T)I - R_L I \tag{3}$$

$$\gamma\frac{dT}{dt} = I^2 R_{tes} - K\left(T^n - T_b^n\right) + \delta P \tag{4}$$

where I and T are the current and temperature of the TES device, R_{tes} and γ are its resistance and heat capacity, L is the inductance in the circuit, $R_L = R_s + R_p$ with R_s and R_p as the bias and parasitic resistance, K and n characterize the heat conduction to the substrate at temperature T_b, and I_b and δP are the bias current and signal power.

In the steady state, the relevant electrical and thermal quantities of the circuit are time-invariant constants. They are obtained by setting the signal power δP and the time derivatives (dI/dt) and (dT/dt) to 0 in (3) and (4). This yields

$$I_b R_s - R_{ss} I_{ss} - R_L I_{ss} = 0 \tag{5}$$

$$I_{ss}^2 R_{ss} - K\left(T_{ss}^n - T_b^n\right) = 0 \tag{6}$$

where I_{ss}, T_{ss}, and $R_{ss} = R_{tes}(I_{ss}, T_{ss})$ are the current, temperature, and resistance of the TES in the steady state. For sophisticated devices with complicated behavior such as the TES, (3) and (4) cannot be analytically solved, and numerical solvers or circuit simulators must be used to determine the dc operating point of the circuit. In circuit simulation, this is called the dc analysis. We have developed device models and simulation techniques to obtain steady states of TES circuits in earlier work [10], [11].

Upon absorption of power δP due to an incident signal, the current and temperature of the TES start to change from their steady-state values. Under the small-signal assumption, they can be written as

$$I(t) = I_{ss} + \delta I(t) \tag{7}$$

$$T(t) = T_{ss} + \delta T(t) \tag{8}$$

where δI and δT are the small response signals that we are interested in. Since the TES resistance is dependent on both the temperature and current of the TES, under small-signal analysis, we can expand it around the steady-state value R_{ss} to first order in δT and δI, i.e.,

$$R_{tes}(T,I) = R_{ss} + \alpha\frac{R_{ss}}{T_{ss}}\delta T + \beta\frac{R_{ss}}{I_{ss}}\delta I \tag{9}$$

with the temperature and current sensitivity defined in (1) and (2). From (3) and (4) and the steady-state condition (5) and (6), we can derive the equations of motion for the small response signals as follows:

$$L\frac{d\delta I}{dt} = -\left(R_L + R_{ss}(1+\beta)\right)\delta I - \alpha\frac{I_{ss}R_{ss}}{T_{ss}}\delta T \tag{10}$$

$$\gamma\frac{d\delta T}{dt} = I_{ss}R_{ss}(2+\beta)\delta I + \left(\alpha\frac{I_{ss}^2 R_{ss}}{T_{ss}} - G\right)\delta T + \delta P. \tag{11}$$

where $G = nKT_{ss}^{n-1}$ is the thermal conductance. These equations can be solved in the time domain to obtain the time dependence of δI and δT. Alternatively, we can also study the problem in the frequency domain by Laplacian transforming (10) and (11) into

$$sL\delta I(s) = -\left(R_L + R_{ss}(1+\beta)\right)\delta I(s) - \alpha\frac{I_{ss}R_{ss}}{T_{ss}}\delta T(s) \tag{12}$$

$$s\gamma\delta T(s) = I_{ss}R_{ss}(2+\beta)\delta I(s) + \left(\alpha\frac{I_{ss}^2 R_{ss}}{T_{ss}} - G\right)\delta T(s) + \delta P(s). \tag{13}$$

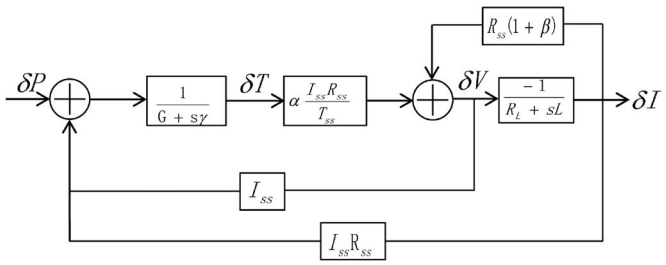

Fig. 3. Block diagram for small-signal analysis of dc-biased TES circuits.

From (12) and (13), we can solve for the transfer function of the system, i.e.,

$$H(s) = \frac{\delta I(s)}{\delta P(s)}. \tag{14}$$

The stability of the circuit is determined by the poles of $H(s)$.

In addition to the analytical method presented above, we can also use the block diagram [12], [13] in Fig. 3 to describe the operation of the circuit and understand the coupling between each part of the system in a visual and intuitive manner. We can clearly see how the electrothermal feedback functions in this diagram and easily derive the system transfer function $H(s)$.

B. IV Relation for TES Devices

The concepts and methods we will introduce for the analysis and simulation of ac-biased TES circuits are generally applicable and do not depend on any specific device model for the TES. Nevertheless, to demonstrate their application in concrete examples, we need to use a particular device model for simulation. In spite of the widespread application of TES, its exact underlying physics is still unresolved, and multiple physical models are used in the literature such as the two-fluid model [14]–[16] and the weak-link model [17]. In this paper, we will use TES device models developed earlier [10], [11] based on the two-fluid theory. All our simulation results are thus within the framework of the two-fluid device model. How well they match the actual behavior of TES circuits depends on how accurately the two-fluid model describes the physics of TES devices, which is an open question subject to further investigation and debate.

In a dc-biased circuit, the TES is limited to the transitional state between the superconducting and normal states. In this case, it can be described as an effective resistance, i.e.,

$$R_{tes} = \frac{V_{tes}}{I_{c0}\left(1 - \frac{T}{T_c}\right)^{\frac{3}{2}} + V_{tes}/(C_R R_n)} \tag{15}$$

where V_{tes} is the voltage across the TES, T and T_c are the temperature and critical temperature of the TES, I_{c0} is the 0-temperature critical current, R_n is the normal-state resistance, and C_R is the ratio of the TES normal current resistance in the transitional state to R_n. In an ac-biased circuit, however, it is inadequate to characterize the electrical behavior of the TES using the effective resistance in (15) because the TES can enter the superconducting state when its current falls below I_c and also the normal state when its temperature rises above T_c (see Fig. 4). As discussed in [11], in this case, we need a more comprehensive IV relation for the TES that takes into account all possible states of the device. Specifically, the comprehensive IV relation of the TES can be expressed as [11]

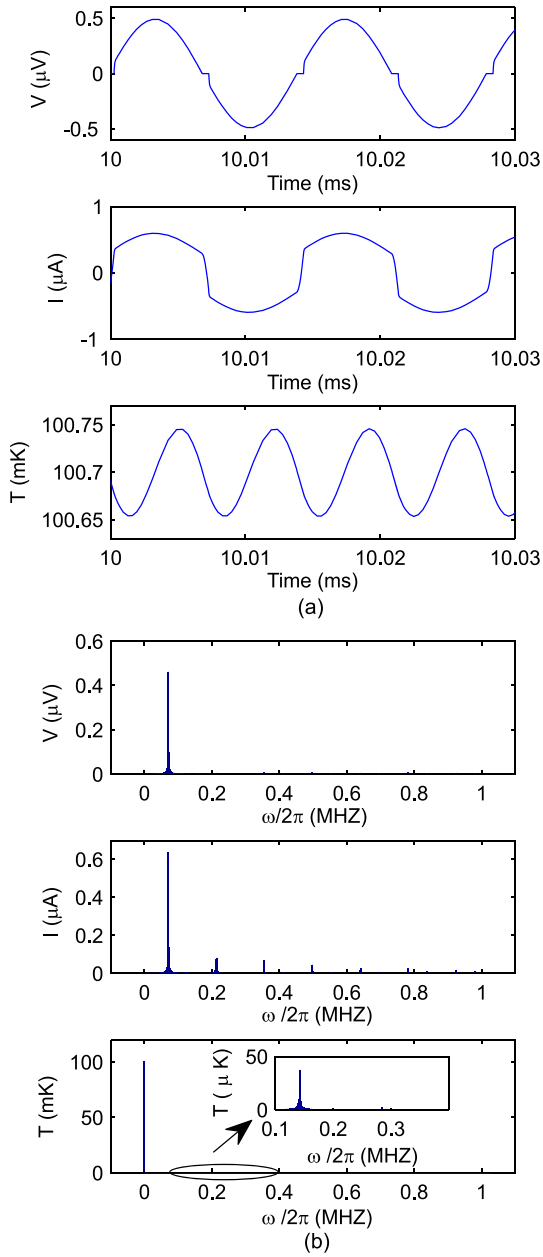

Fig. 4. TES current, voltage, and temperature in the ac-biased circuit in Fig. 1 in the absence of signal power. The amplitude of the bias voltage is 500 nV. (a) Electrical and thermal quantities in the time domain. (b) Spectra of the signals obtained by Fourier transforming the waveforms in (a).

$$\begin{aligned} V_{tes} = {} & \theta(T - T_c) I R_n + \theta(T_c - T)\theta(I - I_c)(I - I_c) C_R R_n \\ & + \theta(T_c - T)\theta(-I - I_c)(I + I_c) C_R R_n \end{aligned} \tag{16}$$

where θ is the step function, and the temperature-dependent critical current $I_c(T)$ is given by the BCS relation, i.e.,

$$I_c = I_{c0}(1 - T/T_c)^{\frac{3}{2}}. \tag{17}$$

We can rewrite (16) in the following slightly more concise form:

$$V_{tes} = \theta(T_c - T)\theta\left(abs(I) - I_c\right)\left(I - sgn(I)I_c\right)C_R R_n + \theta(T - T_c)IR_n \quad (18)$$

where abs and sgn are the absolute-value function and the sign function, respectively. In (16) and (18), the TES current I can be positive or negative depending on its direction. The critical current I_c is taken to be a positive value.

We can use the analog behavioral modeling functionality provided by advanced circuit simulators to build device models for the TES based on the IV relation in (16) or (18). The resulting device models can be further integrated in advanced electronic design automation (EDA) software and tools to modernize the design and simulation workflow of TES circuits. Detailed explanation of how the models are constructed and how they are used in circuit simulation can be found in [11]. In this paper, we use the SpectreRF circuit simulator for our circuit simulation. The analog behavioral TES model for Spectre is shown in Listing 1 in Appendix B.

III. Periodic Steady State

A. Behavior of AC-Biased Circuits Without an Input Signal

From the circuit diagram in Fig. 1, we can write the equations for the electrical and thermal quantities in an ac-biased TES circuit as follows:

$$V_b\cos(\omega_0 t) = V_{tes} + L\frac{dI}{dt} + \frac{1}{C}\int Idt + IR_L \quad (19)$$

$$\gamma\frac{dT}{dt} = IV_{tes} - K\left(T^n - T_b^n\right) + \delta P \quad (20)$$

where C is the capacitance in the circuit, V_b and ω_0 are the amplitude and frequency of the bias voltage, and all other quantities have been defined earlier. The frequency of the bias voltage ω_0 is usually chosen to be the same with the LC resonance frequency $1/\sqrt{LC}$ to increase the TES current. The TES voltage is given by (16) or (18).

The major difficulty in the analysis of ac-biased TES circuits is that all electrical and thermal quantities continuously change even in the absence of an input signal. Consequently, the technique of Taylor expansion around dc steady-state values in small-signal analysis of dc-biased circuits is no longer applicable. It is further complicated by the fact that, due to the highly nonlinear nature of the TES, the current, voltage, and temperature of the TES under the bias of a sinusoidal voltage source of a single frequency ω_0 can have higher-order harmonic terms, which are referred to as harmonic distortion (HD). This can be confirmed by a transient simulation of the ac-biased circuit in the absence of an input signal, which we can perform due to our earlier work [11]. The result [11] is shown in Fig. 4(a). It is clearly seen that the waveforms of the TES current and voltage can deviate from sinusoidal, which implies the existence of higher harmonics. Such deviation can occur because the TES enters the superconducting and 0-voltage state in each cycle of the oscillation when the current drops below its critical current, as shown in the voltage plot in Fig. 4(a). In the superconducting state, the current is solely determined by the load resistance (R_L in Fig. 1), and its waveform follows that of the bias voltage. When the current reverses direction and rises above the critical current again, the TES goes back to the transitional state, where its waveform deviates from that in the superconducting state because of the current-dependent TES resistance, hence the two segments with distinctive characteristics and shapes in each half cycle of the current plot in Fig. 4(a). In Fig. 4(b), the spectra of the electrical and thermal quantities are shown. It is observed that the current and voltage contain odd harmonics of the bias frequency ω_0, whereas the temperature contains even harmonics of ω_0.

B. Concept of Periodic Steady State

In spite of the aforementioned complexity, the current, voltage, and temperature of an ac-biased TES circuit in the absence of an input signal are periodic functions with the same period as the bias voltage. Although the electrical and thermal quantities are continuously changing, such a state of the TES can be conceptually considered a generalized steady state in the sense that it does not change from one period to another. Because of its periodic nature, it is called the "periodic steady state" (PSS) [6]. As will be seen in Section IV, the PSS plays a similar role in the analysis of ac-biased TES circuits as does the dc steady state in small-signal analysis of dc-biased circuits. Technically, the PSS is obtained by setting the input signal power δP to 0 in (19) and (20) and solve for the current, voltage, and temperature of the TES. This is reminiscent of our setting δP to 0 in (3) and (4) and solving for the dc steady state, except that we do not also require (dI/dt) and (dT/dt) to be 0 since the PSS is time dependent within each period. The waveform of the PSS can actually be obtained analytically when the TES is in certain states. For instance, in each cycle of the oscillation, the TES current will drop below the critical current I_c, as shown in Fig. 4(a). When this occurs, the TES enters the superconducting state since $|I| < I_c$. The IV relation in (16) and (18) reduces to $V_{tes} = 0$, and (19) and (20) lead to the following equations for the PSS when the TES is in the superconducting state:

$$V_b\cos(\omega_0 t) = L\frac{dI_{pss}}{dt} + \frac{1}{C}\int I_{pss}dt + I_{pss}R_L \quad (21)$$

$$\gamma\frac{dT_{pss}}{dt} = -K\left(T_{pss}^n - T_b^n\right) \quad (22)$$

where $I_{pss}(t)$ and $T_{pss}(t)$ are the current and temperature of the PSS. These equations are trivial to solve because the electrical and thermal equations are decoupled, and the impedance of the inductance and capacitance cancel each other at the resonant frequency ω_0.

The simplicity of the PSS waveform in certain parts within a period, however, is not an indication that it is good practice to solve for the PSS in the time domain. Not only is it difficult to solve for the PSS analytically in the transitional state of the TES due to electrothermal coupling, but it is also unfeasible to obtain analytical expressions for the times when the TES enters and leaves each of its possible states. Consequently, it is impractical to gain either detailed information or intuitive understanding about the spectrum of the PSS in a time-domain treatment. A conceptually much more revealing approach is to express the

PSS current, voltage, and temperature of the TES as a series of all possible harmonic terms as in the following:

$$I_{pss} = \sum_{m=0}^{\infty} I_{2m+1} \cos\left((2m+1)\omega_0 t + \phi_{I_{2m+1}}\right) \tag{23}$$

$$V_{pss} = \sum_{m=0}^{\infty} V_{2m+1} \cos\left((2m+1)\omega_0 t + \phi_{V_{2m+1}}\right) \tag{24}$$

$$T_{pss} = \sum_{m=0}^{\infty} T_{2m} \cos\left(2m\omega_0 t + \phi_{T_{2m}}\right). \tag{25}$$

In these expressions, we have kept only odd harmonics in the current and voltage and even harmonics in the temperature. The fact that these are the only nonzero terms can be proved by a parity analysis and is confirmed in the simulation result in Fig. 4(b). We can also introduce their complex representation, i.e.,

$$\tilde{I}_{pss} = \sum_{m=0}^{\infty} \tilde{I}_{2m+1} e^{j(2m+1)\omega_0 t} \tag{26}$$

$$\tilde{V}_{pss} = \sum_{m=0}^{\infty} \tilde{V}_{2m+1} e^{j(2m+1)\omega_0 t} \tag{27}$$

$$\tilde{T}_{pss} = \sum_{m=0}^{\infty} \tilde{T}_{2m} e^{j2m\omega_0 t} \tag{28}$$

where $\tilde{I}_{2m+1} = I_{2m+1} e^{j\phi_{I_{2m+1}}}$, $\tilde{V}_{2m+1} = V_{2m+1} e^{j\phi_{V_{2m+1}}}$, and $\tilde{T}_{2m} = T_{2m} e^{j\phi_{T_{2m}}}$. In (26)–(28) and the rest of this paper, we use the tilde to indicate a complex quantity that has both an amplitude and a phase.

Equations (23)–(28) can then be substituted into (19), (20), and (16) or (18) to derive the following equations:

$$\sum_m \left\{\tilde{I}_{2m+1}\tilde{Z}_{RLC}\left((2m+1)\omega_0\right) + \tilde{V}_{2m+1} - V_b\delta_{m,0}\right\} \times e^{j(2m+1)\omega_0 t} = 0 \tag{29}$$

$$\sum_m 2m\omega_0\gamma T_{2m}\sin\left(2m\omega_0 t + \phi_{T_{2m}}\right) + \sum_m I_{2m+1}\cos\left((2m+1)\omega_0 t + \phi_{I_{2m+1}}\right) \cdot \sum_l V_{2l+1}\cos\left((2l+1)\omega_0 t + \phi_{V_{2l+1}}\right) = K\left[\left(\sum_m T_{2m}\cos\left(2m\omega_0 t + \phi_{T_{2m}}\right)\right)^n - T_b^n\right] \tag{30}$$

$$V_{tes}\left(\sum_m I_{2m+1}\cos\left((2m+1)\omega_0 t + \phi_{I_{2m+1}}\right), \sum_m T_{2m}\cos\left(2m\omega_0 t + \phi_{T_{2m}}\right)\right) = \sum_m V_{2m+1}\cos\left((2m+1)\omega_0 t + \phi_{V_{2m+1}}\right) \tag{31}$$

where the impedance, i.e.,

$$\tilde{Z}_{RLC}(\omega) = R_L + j\omega L + \frac{1}{j\omega C} \tag{32}$$

and $V_{tes}(I,T)$ is the expression on the right-hand side of (16) or (18). Since $e^{jm\omega_0 t}$ is a set of linearly independent functions over a period $T = 2\pi/\omega_0$, we can conclude from (29) that

$$\tilde{I}_{2m+1}\tilde{Z}_{RLC}\left((2m+1)\omega_0\right) + \tilde{V}_{2m+1} - V_b\delta_{m,0} = 0 \tag{33}$$

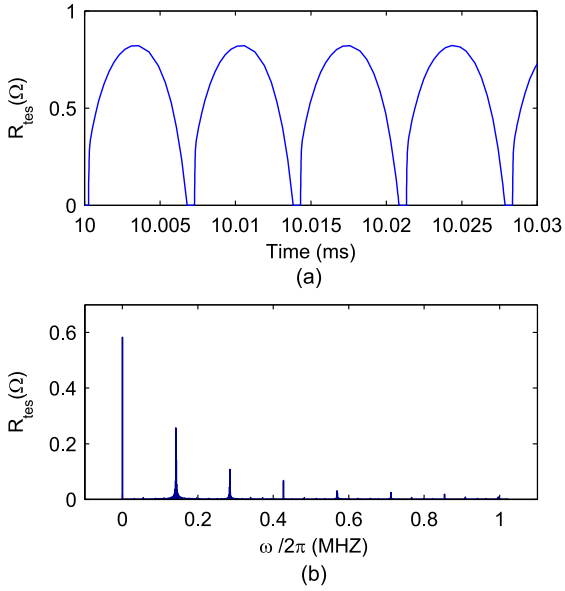

Fig. 5. DC resistance of the TES (defined as V_{tes}/I_{tes}) in the ac-biased TES circuit in Fig. 1. (a) Resistance is plotted in the time domain. (b) Its spectrum is shown.

for each m. This method of solving for the PSS is referred to as harmonic balance [6]. Obviously, in principle, (30) and (31) can be written in a series of even and odd harmonic terms similar to (29), although explicit expressions are not easy to obtain due to the complexity of the IV relation and the dependence of the heat conduction on the TES temperature. By the same argument of harmonic balance, we can derive two more sets of equations involving I_{2m+1}, V_{2m+1}, and T_{2m} similar to (33) for each harmonic m. These equations can then be solved to determine the coefficients I_{2m+1}, V_{2m+1}, and T_{2m} and, thus, the PSS.

In Fig. 4, we have calculated the PSS of the ac-biased TES circuit using a transient circuit simulation. Although such a familiar time-domain simulation technique seems natural for the purpose of determining the PSS, it is actually very inefficient from a computational point of view [6]. This is because much of the computer time is spent on the calculation of the expected and uninteresting oscillation driven by the ac bias voltage. When the frequency of the bias voltage is high or when there is significant HD, the time step of the transient simulation must be very small to ensure the accuracy of the simulation. In contrast, the harmonic balance equations resulting from (29)–(31) can be solved much more efficiently using standard numerical algorithms such as Newton's method [6] without time-domain transient simulation. (To make the problem tractable, only coefficients up to a certain harmonic are kept.) Therefore, the introduction of the PSS not only clarifies our understanding of the steady-state behavior of ac-biased circuits but also improves the efficiency of circuit simulation dramatically. It is a key concept for the analysis of ac-biased circuits for these reasons.

C. Application of PSS Simulation

A few advanced circuit simulators that support RF circuit design provide built-in functionality for PSS simulation that can be used to determine the PSS of ac-biased circuits. (Not all

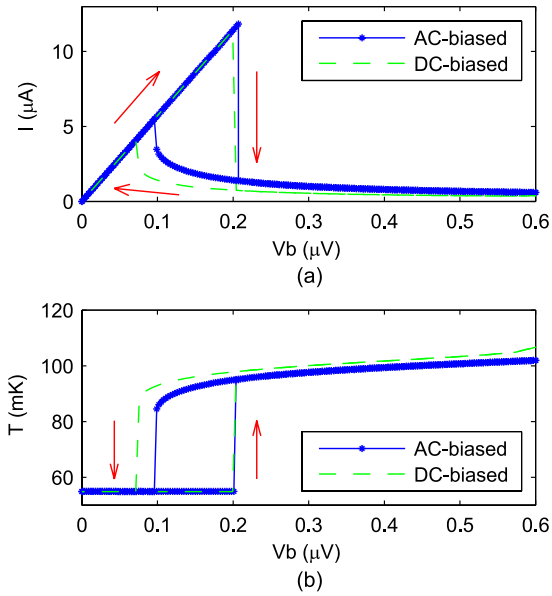

Fig. 6. Fundamental-frequency current [I_1 in (23)] and dc temperature [T_0 in (25)] of the PSS for the ac-biased TES circuit in Fig. 1 as a function of the ac bias voltage. The simulation file is shown in Listing 3 in Appendix B. Moreover, plotted for comparison are the results of dc analysis [11] of a dc-biased circuit in Fig. 2 with the same TES device and load resistance ($V_b = I_b R_s$ for the dc-biased circuit).

simulators support PSS simulation, though. The popular Pspice for use on desktop computers, for example, does not support PSS simulation.) In our work, we use the SpectreRF simulator for PSS simulation. The device model and simulation files are included in the Appendix.

By using PSS simulation, we can study the behavior of ac-biased TES circuits in great detail and gain valuable insights directly relevant to experiments. For instance, in dc-biased circuits, IV curve measurement is often used to characterize the TES device and establish the dc operating point. In ac-biased circuits, one can use a similar approach to measure how the effective TES current changes with the amplitude of the ac bias voltage V_b. Although, it is much harder to conceptually deduce every detail of the IV curve, because the TES can alternate between the superconducting and transitional states, and HD exists in the circuit. PSS simulation is a perfect tool to study this problem. In Fig. 6, the fundamental-frequency current and dc temperature of the TES in the ac-biased circuit in Fig. 1 are obtained in a PSS simulation and plotted against the amplitude of the ac bias voltage. Interestingly, the curves exhibit a hysteresis much like the (dc) TES current and temperature in a dc-biased circuit [10], [11], which are also plotted for comparison. It indicates that the transition from and to the superconducting state occurs at different bias points when the bias voltage is increased and decreased as observed in experiments [19]. In Fig. 6, the superconducting branches of the ac- and dc-biased circuits overlap, since the slope is solely determined by the load resistance. The resistive branches, however, are somewhat different, suggesting that the effective resistance of the fundamental-frequency current is different from the TES resistance in a dc-biased circuit.

Previously, when rigorous understanding of ac-biased TES circuits was lacking and simulation tools to accurately predict

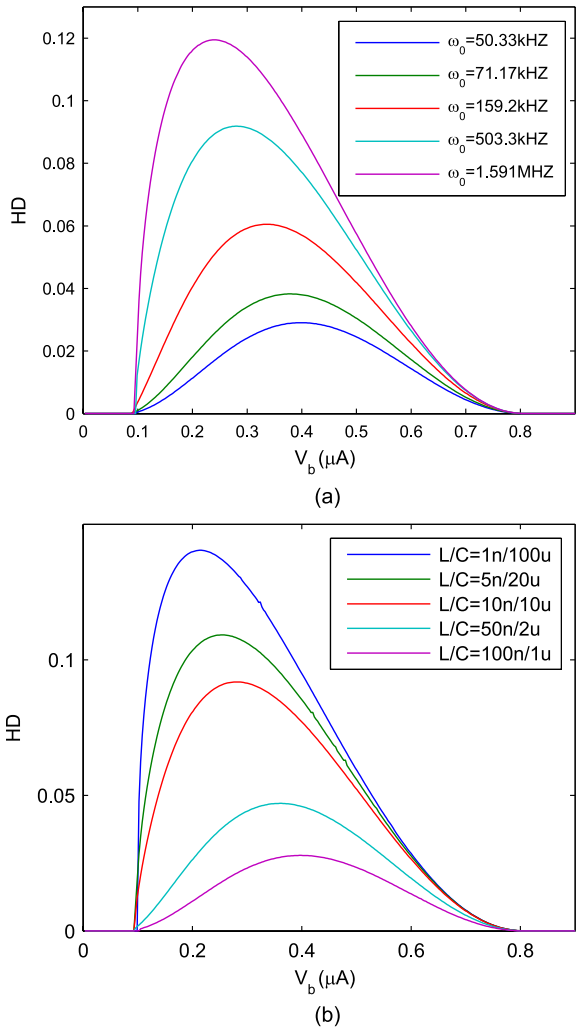

Fig. 7. HD of the ac-biased TES circuit in Fig. 1. (a) HD under different carrier frequencies. The bias voltage V_b is swept from high to low (which is different than from low to high because of the hysteresis in Fig. 6). The frequency is adjusted by fixing the capacitance at $C = 10$ μF and changing the value of the inductance. (b) Dependence of the HD on the Q-factor of the circuit. The carrier frequency is fixed at 503.3 kHz. The Q-factor is tuned by changing the values of the capacitance and inductance while keeping their product fixed (such that the resonant frequency $\omega_0 = 1/\sqrt{LC}$ is fixed).

their behavior were unavailable, people often relied on concepts and formulas from the study of dc-biased circuits for approximate analysis of ac-biased circuits. A common problem of such crude manual analysis is that there is no way to reliably evaluate the effect of nonlinearity of the TES, which is important at high carrier frequencies targeted by the large-scale application of TES arrays. With the help of PSS simulation, we can accurately gauge how much HD is in the circuit and observe how it depends on the circuit parameters and bias conditions. It is even possible to optimize the circuit design based on the simulation results. In Fig. 7(a), we plot the HD, which is defined as the power ratio between higher harmonics and the fundamental-frequency component, $\sum_{m>0} |I_{2m+1}|^2/|I_1|^2$, under different frequencies of the bias voltage. We see that the HD is 0 when the TES is in the superconducting (when V_b is small) and normal states (when V_b is large) and nonzero in the transitional state. Moreover, the HD becomes more severe

when the bias frequency increases. Because of this, it may pose a challenge to operating ac-biased TES circuits at high carrier frequencies, depending on the technical specification of the design requirement. In Fig. 7(b), we plot the HD under the same carrier frequency but with different values of L and C. In effect, by keeping the product of L and C fixed, the Q-factor of the circuit is tuned. It is observed that circuits with a higher Q-factor have lower HD, which is valuable information for circuit design. Although, it does not necessarily mean that the circuit's Q-factor should be maximized, because there are other design considerations at work such as desired signal levels and practical parameter ranges.

As indicated in Fig. 7, the HD of ac-biased TES circuits is sensitive to factors such as device parameters and bias conditions, which is a common feature of nonlinear RF circuits. It can potentially cause contamination in frequency regions above the first harmonic, which is harmful for FDM if the relevant working conditions of the circuit are not set properly. Nevertheless, it is possible to choose appropriate parameter values and bias conditions to obtain an ac-biased TES circuit with minimized HD and, thus, approximately linear response. PSS analysis is a powerful tool for this purpose. Careful circuit simulation based on it can greatly help understand the complexity involved in the circuit design and be used to engineer proper solutions and meet the challenges in suppressing the HD.

IV. Periodic AC Analysis

A. Response to Small Input Signal

Once the PSS of an ac-biased TES circuit is determined, we next study how it responds to external input signals. If the input signal power δP is sufficiently small, it is reasonable to assume that the current and temperature of the TES, i.e., $I(t)$ and $T(t)$, only deviate from the steady-state values $I_{pss}(t)$ and $T_{pss}(t)$ by a small amount. This consideration leads to

$$I(t) = I_{pss}(t) + \delta I(t) \tag{34}$$

$$T(t) = T_{pss}(t) + \delta T(t) \tag{35}$$

where $\delta I(t)$ and $\delta T(t)$ are the small deviation from the PSS values due to the signal power δP. They are the response signals that we are interested in. Conceptually, (34) and (35) should be related to (7) and (8) in small-signal analysis of dc-biased circuits, except that the PSS is time dependent.

Because of the small changes in current and temperature, i.e., δI and δT, there will also be a small change δV in the TES voltage, leading to

$$V_{tes}(t) = V_{pss}(t) + \delta V(t). \tag{36}$$

By parallelism to analysis of dc-biased TES circuits, one might be tempted to define the dc resistance, i.e.,

$$R_{pss}(t) = \frac{V_{pss}(t)}{I_{pss}(t)} \tag{37}$$

and its temperature and current sensitivity, i.e.,

$$\alpha = \frac{T_{pss}}{R_{pss}} \frac{\partial R}{\partial T}\bigg|_{I_{pss}}, \ \beta = \frac{I_{pss}}{R_{pss}} \frac{\partial R}{\partial I}\bigg|_{T_{pss}}. \tag{38}$$

However, it is easily seen that such an approach is problematic, both conceptually and in practice. As shown in Fig. 5, the dc resistance of the TES in an ac-biased circuit is time dependent. This time dependence cannot be neglected because the swing of the TES resistance is always comparable to its dc component since the TES will enter the superconducting state in each cycle of the oscillation. Consequently, the temperature and current sensitivities defined in (38) are necessarily time dependent. Worse, when the TES is in the superconducting state, its resistance is 0, and the definition in (38) becomes meaningless (as a matter of fact, the TES is not sensitive to changes in temperature and current in the superconducting state). Considering these difficulties, we directly make a variational expansion of the TES voltage with respect to the TES current and temperature around the PSS value V_{pss}, i.e.,

$$V_{tes} = V_{pss} + \Omega \delta I + \Lambda \delta T \tag{39}$$

where

$$\Omega(t) = \frac{\partial V_{tes}}{\partial I}\bigg|_{T_{pss}} \tag{40}$$

$$\Lambda(t) = \frac{\partial V_{tes}}{\partial T}\bigg|_{I_{pss}}. \tag{41}$$

Notice that, because of the periodic nature of the PSS, R_{pss}, Ω, and Λ defined in (37), (40), and (41) are also periodic. It can be further deduced that they contain only even and odd harmonics of ω_0. Their complex representations are

$$\tilde{R}_{pss} = \sum_{m=0}^{\infty} \tilde{R}_{2m} e^{j2m\omega_0 t} \tag{42}$$

$$\tilde{\Omega} = \sum_{m=0}^{\infty} \tilde{\Omega}_{2m} e^{j2m\omega_0 t} \tag{43}$$

$$\tilde{\Lambda} = \sum_{m=0}^{\infty} \tilde{\Lambda}_{2m+1} e^{j(2m+1)\omega_0 t}. \tag{44}$$

Ω and Λ can be calculated according to the TES IV relation (16) or (18). As can be seen in Fig. 4, T_{pss} has a large dc value T_0 close to T_c and much smaller even-order harmonic terms. If the input signal power is not too high, the temperature of the TES, which is close to T_{pss}, will always remain below T_c. This is the desired working region to obtain strong electrothermal feedback. Under these conditions, we have [11]

$$\Omega = \left[\theta(I_{pss} - I_s) + \theta(-I_{pss} - I_s)\right] C_R R_n \tag{45}$$

$$\Lambda = \frac{1.5 I_s}{T_c - T_{pss}} \left[\theta(I_{pss} - I_s) - \theta(-I_{pss} - I_s)\right] C_R R_n. \tag{46}$$

Physically, these equations simply state that the TES voltage is dependent on the TES current and temperature only when the TES current is above the critical current. The waveforms and spectra of Ω and Λ are shown in Fig. 8. In comparison to the dc resistance defined in (37) and plotted in Fig. 5, we see that the waveform of Ω is much simpler. Its physical meaning is also very clear in that it characterizes the resistance of the normal current when the TES is in the transitional state and becomes 0 when the TES enters the superconducting state. For these

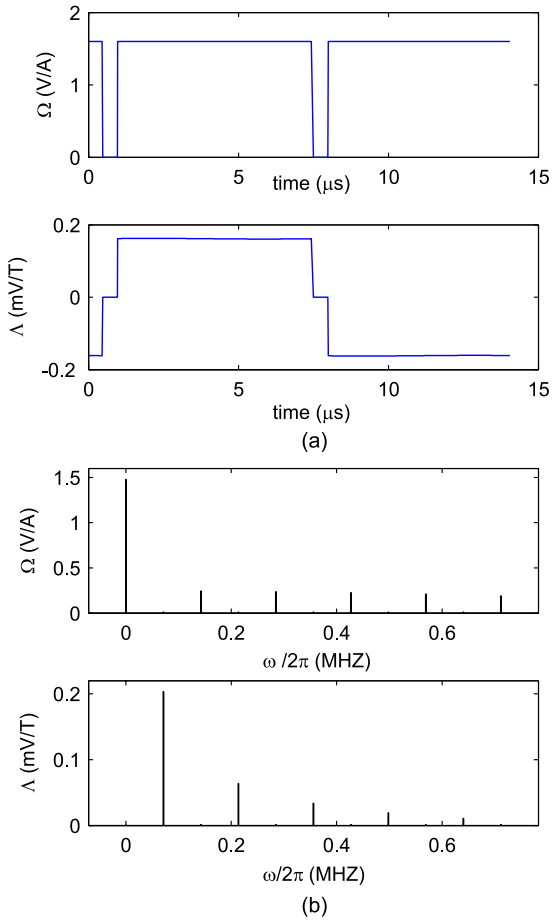

Fig. 8. (a) Waveforms in one period and (b) spectra of Ω and Λ for the ac-biased TES circuit in Fig. 1.

reasons, it is a much more convenient and revealing quantity for studying the small-signal response of ac-biased TES circuits.

Substituting (34)–(36) into (19) and (20) and making use of the equations that $I_{pss}(t)$ and $T_{pss}(t)$ satisfy, we can derive the following equations for the response signals $\delta I(t)$ and $\delta T(t)$:

$$L\frac{d\delta I}{dt} + \frac{1}{C}\int \delta I dt + (R_L + \Omega)\delta I + \Lambda \delta T = 0 \tag{47}$$

$$\gamma \frac{d\delta T}{dt} = I_{pss}(\Lambda \delta I + \Omega \delta T) + V_{pss}\delta I - G\delta T + \delta P \tag{48}$$

where we have kept only terms to first order in δI and δT, and $G = nKT_{pss}^{n-1}$ is the heat conductance evaluated at T_{pss}. In these equations, I_{pss} and T_{pss} should be considered known functions of time (obtained from the PSS analysis). Equations (47) and (48) are the equivalent of (10) and (11) in the analysis of ac-biased TES circuits. Unlike in dc-biased circuits, G, Ω, and Λ are all time dependent.

Considering the step functions in (45) and (46), we can discuss the behavior of δI and δT in the superconducting and transitional states of the TES separately. In the superconducting state $-I_c < I_{pss} < I_c$, (47) and (48) simplify to

$$L\frac{d^2\delta I}{dt^2} + R_L\frac{d\delta I}{dt} + \frac{1}{C}\delta I = 0 \tag{49}$$

$$\gamma \frac{d\delta T}{dt} = -G\delta T + \delta P. \tag{50}$$

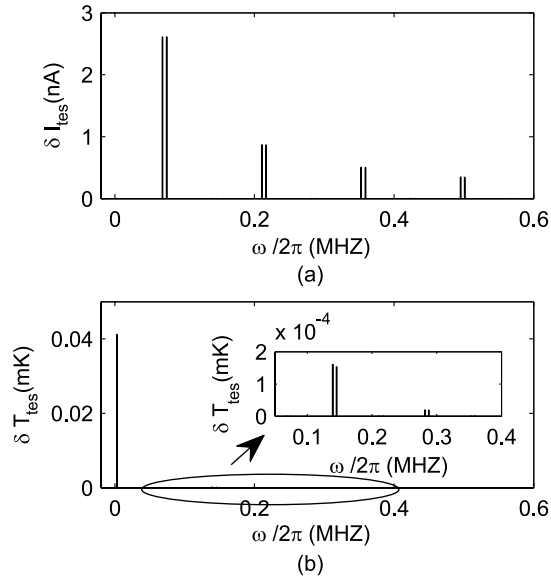

Fig. 9. Sidebands in the spectra of the TES small-signal response. The frequency of the input signal is 3 KHz. (a) Spectrum of δI. Upper and lower sidebands at odd harmonics of ω_0 are present. The carrier frequency ω_0 is about 71 KHz. (b) Spectrum of δT. Upper and lower sidebands at even harmonics of ω_0 are present.

These equations are decoupled and very easy to solve. δI has a damped oscillation at frequency $\omega_0 = 1/\sqrt{LC}$ that decays at a rate determined by R_L. δT has an exponential decay at the intrinsic thermal rate G/γ, which is slow since electrothermal feedback is not at work.

When the TES is in the transitional state $I_{pss} > I_c$, (47) and (48) become

$$L\frac{d^2\delta I}{dt^2} + (R_L + C_R R_n)\frac{d\delta I}{dt} + \frac{1}{C}\delta I + \frac{1.5 I_c C_R R_n}{T_c - T_{pss}}\frac{d\delta T}{dt} = 0 \tag{51}$$

$$\gamma \frac{d\delta T}{dt} = (V_{pss} + I_{pss}C_R R_n)\delta I + \left(\frac{1.5 I_c C_R R_n}{T_c - T_{pss}} I_{pss} - G\right) \times \delta T + \delta P. \tag{52}$$

Similar equations result when the current is in the other direction, i.e., $I_{pss} < -I_c$. These equations are coupled, and they cannot be analytically solved because of the complicated time dependence of V_{pss}, I_{pss}, T_{pss}, I_c, and G. Nevertheless, it can be seen how the thermal and electrical quantities are coupled because of the electrothermal feedback. The electrical and thermal behavior of the TES in the transitional state in ac-biased circuits is complicated because the electrothermal feedback is time dependent.

B. Periodic AC Analysis

A better approach to solving (47) and (48) is in the frequency domain. Since these small-signal equations are linear (but not time invariant as the small-signal equations for dc-biased circuits), we can study how the circuit responds to a small sinusoidal input signal, i.e.,

$$\delta P = A\cos(\omega t) \tag{53}$$

and use the principle of superposition to determine its response to a signal of finite bandwidth. By analogy to ac analysis in dc-biased circuits, this is called a "periodic ac analysis" (PAC).

Under an ac stimulus in (53), since I_{pss} and T_{pss} have odd and even harmonics of ω_0, the response δI and δT will have upper and lower sidebands at each of these harmonics, as shown in Fig. 9. We can then write the solution in the following form (neglecting smaller higher-order sidebands at $m\omega_0 \pm l\omega$ with $|l| > 1$):

$$\delta I = \sum_{m=0}^{\infty} \delta I_{(2m+1)L} \cos\left[((2m+1)\omega_0 - \omega)\, t + \phi_{\delta I_{(2m+1)L}}\right] + \sum_{m=0}^{\infty} \delta I_{(2m+1)U} \cos\left[((2m+1)\omega_0 + \omega)\, t + \phi_{\delta I_{(2m+1)U}}\right] \tag{54}$$

$$\delta T = \sum_{m=1}^{\infty} \delta T_{2mL} \cos\left((2m\omega_0 - \omega)t + \phi_{\delta T_{2mL}}\right) + \sum_{m=0}^{\infty} \delta T_{2mU} \cos\left((2m\omega_0 + \omega)t + \phi_{\delta T_{2mU}}\right) \tag{55}$$

where $\delta I_{(2m+1)L}$, $\delta I_{(2m+1)U}$, δT_{2mL}, δT_{2mU}, $\phi_{\delta I_{(2m+1)L}}$, $\phi_{\delta I_{(2m+1)U}}$, $\phi_{\delta T_{2mL}}$, and $\phi_{\delta T_{2mU}}$ are the upper and lower sideband amplitude and phase at corresponding harmonics of ω_0. The complex representation is

$$\delta\tilde{I} = \sum_{m=0}^{\infty} \delta\tilde{I}_{(2m+1)L} e^{j((2m+1)\omega_0 - \omega)t} + \sum_{m=0}^{\infty} \delta\tilde{I}_{(2m+1)U} e^{j((2m+1)\omega_0 + \omega)t} \tag{56}$$

$$\delta\tilde{T} = \sum_{m=1}^{\infty} \delta\tilde{T}_{2mL} e^{j(2m\omega_0 - \omega)t} + \sum_{m=0}^{\infty} \delta\tilde{T}_{2mU} e^{j(2m\omega_0 + \omega)t} \tag{57}$$

where $\delta\tilde{I}_{(2m+1)L} = \delta I_{(2m+1)L} e^{j\phi_{\delta I_{(2m+1)L}}}$, $\delta\tilde{I}_{(2m+1)U} = \delta I_{(2m+1)U} e^{j\phi_{\delta I_{(2m+1)U}}}$, $\delta\tilde{T}_{2mL} = \delta T_{2mL} e^{j\phi_{\delta T_{2mL}}}$, and $\delta\tilde{T}_{2mU} = \delta T_{2mU} e^{j\phi_{\delta T_{2mU}}}$.

Substituting (23)–(28), (43), (44), and (54)–(57) into (47) and (48), we then obtain a set of equations containing harmonic terms at all harmonic sidebands $m\omega_0 \pm \omega$. By the principle of harmonic balance, the coefficients of each $e^{j(m\omega_0 \pm \omega)t}$ term must be 0, resulting in a set of equations that can be used to solve for $\delta\tilde{I}_{(2m+1)L}$, $\delta\tilde{I}_{(2m+1)U}$, $\delta\tilde{T}_{2mL}$, and $\delta\tilde{T}_{2mU}$ and, thus, determine the PAC response δI and δT. Because of the complexity of these equations, we list them in Appendix A. Here, we only give the equations for $\delta\tilde{T}_{0U}$, $\delta\tilde{I}_{1L}$, and $\delta\tilde{I}_{1U}$, which are the quantities of the most interest. They are derived from the thermal equation at the base upper sideband (of frequency ω) and the electrical equations at the fundamental upper and lower sidebands (of frequencies $\omega_0 \pm \omega$) by keeping only leading order terms. They are in the following form:

$$\left[(G_0 + j\omega\gamma) - \frac{1}{4}\left(\tilde{\Lambda}_1^* \tilde{I}_1 + \tilde{\Lambda}_1 \tilde{I}_1^*\right)\right] \delta\tilde{T}_{0U} - \frac{1}{2}\left[(\tilde{V}_1 + \Omega_0 \tilde{I}_1)\delta\tilde{I}_{1L}^* + \left(\tilde{V}_1^* + \Omega_0 \tilde{I}_1^*\right)\delta\tilde{I}_{1U}\right] = A \tag{58}$$

$$\left[\tilde{Z}_{RLC}(\omega_0 + \omega) + \Omega_0\right]\delta\tilde{I}_{1U} + \frac{1}{2}\tilde{\Lambda}_1 \delta\tilde{T}_{0U} = 0 \tag{59}$$

$$\left[\tilde{Z}_{RLC}(\omega_0 - \omega)^* + \Omega_0\right]\delta\tilde{I}_{1L}^* + \frac{1}{2}\tilde{\Lambda}_1^* \delta\tilde{T}_{0U} = 0 \tag{60}$$

where $\tilde{I}_1$ and $\tilde{V}_1$ are the (complex) fundamental-frequency component of the PSS, Ω_0 and $\tilde{\Lambda}_1$ are the dc and fundamental-frequency component in (43) and (44), $\tilde{Z}_{RLC}$ is defined in (32), and $G_0 = nKT_0^{n-1}$ with T_0 as the dc component of T_{pss}.

C. TES Sensitivity and Transfer Functions

Although we have performed a rigorous analysis of ac-biased TES circuits, the complicated math makes the treatment less intuitive. It would be very helpful if we could understand and visualize the interaction and feedback between the electrical and thermal quantities using concepts and techniques from the study of dc-biased circuits. This is possible to a certain extent.

Conceptually, the frequency domain (58)–(60) should be compared with (12) and (13) for dc-biased circuits, with the important distinction that (12) and (13) are universal in the analysis of dc-biased circuits, whereas (58)–(60) only apply to the lowest order $(m = 0)$ harmonic sidebands in the analysis of ac-biased circuits. A more visual approach is to compare the block diagram in Fig. 10 for the base frequency upper sideband ($e^{j\omega t}$ terms) power in an ac-biased circuit to the block diagram for a dc-biased circuit in Fig. 3. Such a comparison suggests that we can relate $\tilde{\Lambda}$ in Fig. 10 to $(\alpha I_{ss} R_{ss})/T_{ss}$ in Fig. 3. If we further relate T_0, the dc component of the PSS temperature in (28), R_0, the dc component of the PSS resistance in (42), and $\tilde{I}_1$, the fundamental-frequency component of the PSS current in (26), to steady-state values T_{ss}, R_{ss}, and I_{ss} in dc-biased circuits, we then arrive at the following effective definition for temperature sensitivity:

$$\alpha_{ac} = \frac{T_0}{R_0}\frac{\tilde{\Lambda}_1}{\tilde{I}_1}. \tag{61}$$

In Fig. 10, it is seen that it characterizes the sensitivity of the TES voltage response at the fundamental-frequency sidebands with respect to the variation of the base upper sideband of the temperature, i.e., $\delta\tilde{T}_{0U}$. Using the definition of $\Lambda(t)$ in (41), we can express α_{ac} in terms of the dc resistance $R_{pss}(t)$ defined in (37), i.e.,

$$\alpha_{ac} = \frac{T_0}{R_0}\left\langle \frac{\partial R_{pss}}{\partial T} \right\rangle \tag{62}$$

which has the same form with the definition in [5] except that $\langle \partial R_{pss}/\partial T \rangle$ is the dc component or cycle-averaged value of $\partial R_{pss}(t)/\partial T$ in the PSS, which may contain higher harmonics when the HD of the circuit is nonnegligible. Although, in [5], α_{ac} was defined only for the first-order response of the circuit,

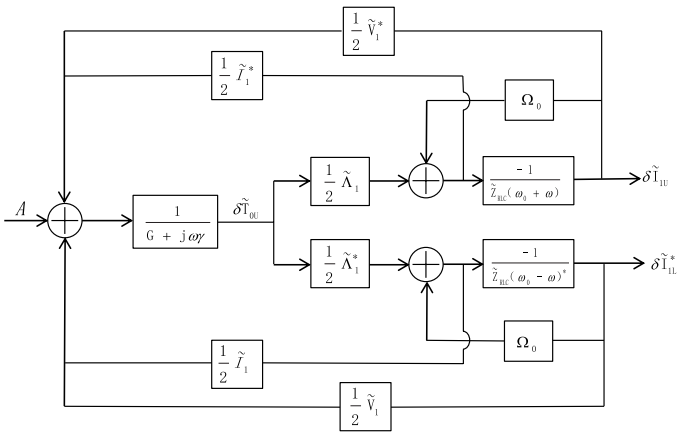

Fig. 10. Block diagram for the base frequency upper sideband ($e^{j\omega t}$) power in the ac-biased TES circuit in Fig. 1.

as shown in Appendix A, it, in fact, characterizes the temperature sensitivity also in higher-order responses. Specifically, for the mth harmonic, α_{ac} describes how sensitive the sideband TES voltage response is to the variation of the mth harmonic sidebands of the temperature, i.e., $\delta\tilde{T}_{2mU}$ and $\delta\tilde{T}_{2mL}$. This fact has its root in the frequency translation behavior of ac-biased nonlinear circuits.

Likewise, we can formally define the effective current sensitivity as

$$\beta_{ac} = \frac{\Omega_0}{R_0} - 1. \tag{63}$$

In terms of the TES resistance $R_{pss}(t)$, it can be shown that

$$\beta_{ac} = \frac{T_0}{R_0}\left\langle \frac{\partial R_{pss}}{\partial I} \right\rangle \tag{64}$$

where $\langle \partial R_{pss}/\partial I \rangle$ is the dc component or the cycle-averaged value of $\partial R_{pss}(t)/\partial I$ in the PSS.

We can calculate the transfer functions, i.e.,

$$H_{1L}(\omega) = \frac{\delta\tilde{I}_{1L}}{A} \tag{65}$$

$$H_{1U}(\omega) = \frac{\delta\tilde{I}_{1U}}{A} \tag{66}$$

from (58)–(60) or by using Fig. 10. Conceptually, (65) and (66) should be considered the counterpart of (14) in dc-biased circuits. The difference is, in ac-biased circuits, there are many more transfer functions because of the frequency translation. These transfer functions need to be labeled by both the harmonic and the sideband. Generally speaking, the transfer functions $H_{(2m+1)U}(\omega)$ and $H_{(2m+1)L}(\omega)$ are evaluated at the frequency $(2m+1)\omega_0 \pm \omega$. They can be calculated using the harmonic balance equations listed in Appendix A.

With the definition of effective temperature and current sensitivities in (61) and (63), one is tempted to evaluate the relative performance of ac- and dc-biased TES circuits by simply comparing their temperature sensitivities. This is a somewhat naive idea, which likely will not lead to sensible conclusions, because ac- and dc-biased circuits are subject to different technical requirements, and they are optimized under different device parameters and working conditions. It is further complicated by other practical issues such as the acceptable level of HD. Considering the complexity involved, a successful design of an ac-biased TES circuit is most likely a tradeoff weighing several relevant factors. The methods and tools introduced can tremendously help in such work. Unfortunately, our current device model does not include noise. Investigation of the performance limit of ac-biased TES circuits will need to be performed in the future.

D. PAC Simulation

Although we have derived the PAC equations for $\delta\tilde{I}$ and $\delta\tilde{T}$ to arbitrary harmonic, they are tedious to solve in practice. Fortunately, advanced circuit simulators with RF simulation capabilities support PAC simulations directly. In Fig. 11, the result of a PAC simulation is plotted. In this simulation, the frequency of the input signal, i.e., ω, is swept at different harmonic m values, and a curve is obtained for each m value. Obviously, its magnitude and phase specify the transfer functions $H_{(2m+1)U}(\omega)$ and $H_{(2m+1)L}(\omega)$. By checking the result of PAC simulation, we can see what the fundamental-frequency sideband components are and how much higher harmonic sideband components are present. As in the application of PSS simulation, we can quantitatively and accurately evaluate important design issues and optimize the circuit by observing how the simulation results change with circuit parameters and bias conditions. Such powerful capability not available before will not only give a huge boost to the design efficiency and reliability but also have a profound impact on experiments.

V. Conclusion

We have presented a rigorous analysis of ac-biased TES circuits that have important applications in FDM of TES detector arrays. We specified the characteristics of the PSS and explained how it is determined from the principle of harmonic balance. We introduced PAC and demonstrated how it is performed to calculate the small-signal response of ac-biased TES circuits. We further used SpectreRF to simulate ac-biased TES circuits and discussed important design issues not addressable before such as the HD. To make our treatment easy to understand, we made connections to the analysis of dc-biased circuits and elucidated how the TES sensitivity in ac-biased circuits should be defined. To our best knowledge, it is the first time that these concepts and techniques are introduced to the study of ac-biased TES circuits. Our work lays a rigorous ground for correct understanding of ac-biased TES circuits and provides a powerful tool to accurately predict their behavior.

Appendix A
Harmonic Balance Equations for PAC Analysis

In Section IV-B, we explained how to solve for the small-signal response $\delta I(t)$ and $\delta T(t)$ to a small single-frequency input signal $A\cos(\omega t)$ in a PAC analysis using the principle of harmonic balance. We list the resulting harmonic balance equations here and demonstrate how to obtain approximate solutions.

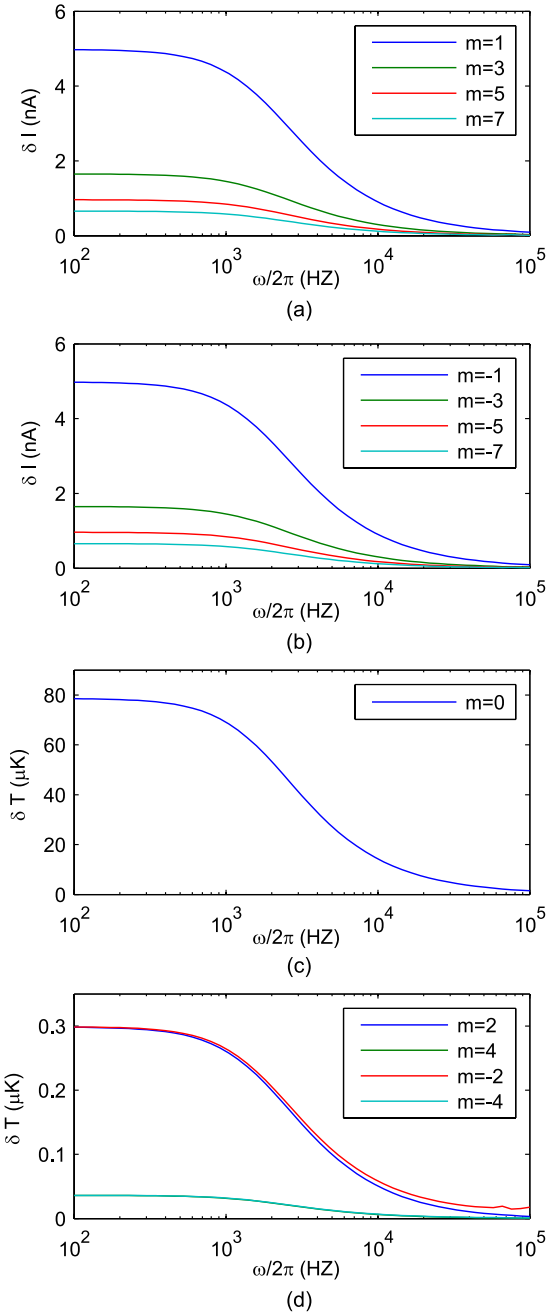

Fig. 11. PAC simulation of the ac-biased TES circuit in Fig. 1. The power of the input sinusoidal signal is 3fW. The simulation file is shown in Listing 4 in Appendix B. (a) Upper-sideband current response. (b) Lower-sideband current response. (c) Temperature response at upper sideband to dc. (d) Upper and lower sideband temperature response at higher harmonics.

The harmonic balance equation for the power at the upper sideband of the mth $(m \geq 0)$ harmonic, which has the frequency $2m\omega_0 + \omega$, is

$$
\begin{aligned}
&j(2m\omega_0+\omega)\gamma\delta\tilde{T}_{2mU} \\
&\quad+\frac{1}{2}\left(\sum_{l=0}^{m}\tilde{G}_{2m-2l}\delta\tilde{T}_{2lU}+\sum_{l=1}^{\infty}\tilde{G}_{2m+2l}\delta\tilde{T}^*_{2lL}\right. \\
&\qquad\left.+\sum_{l=m}^{\infty}\tilde{G}^*_{-2m+2l}\delta\tilde{T}_{2lU}\right) \\
&\quad-\frac{1}{2}\left(\sum_{l=0}^{m-1}\tilde{V}_{2m-2l-1}\delta\tilde{I}_{(2l+1)U}+\sum_{l=0}^{\infty}\tilde{V}_{2m+2l+1}\delta\tilde{I}^*_{(2l+1)L}\right. \\
&\qquad\left.+\sum_{l=m}^{\infty}\tilde{V}^*_{-2m+2l+1}\delta\tilde{I}_{(2l+1)U}\right) \\
&\quad-\frac{1}{4}\left(\sum_{k=0}^{m-1}\sum_{l=0}^{k}\tilde{I}_{2m-2k-1}\tilde{\Omega}_{2k-2l}\delta\tilde{I}_{(2l+1)U}\right. \\
&\qquad+\sum_{k=-l}^{m}\sum_{l=0}^{\infty}\tilde{I}_{2m-2k+1}\tilde{\Omega}_{2k+2l}\delta\tilde{I}^*_{(2l+1)L} \\
&\qquad+\sum_{k=-l}^{-m}\sum_{l=0}^{\infty}\tilde{I}^*_{-2m-2k+1}\tilde{\Omega}^*_{2k+2l}\delta\tilde{I}_{(2l+1)U} \\
&\qquad+\sum_{k=\max(-l,1-m)}^{\infty}\sum_{l=0}^{\infty}\tilde{I}_{2m+2k-1}\tilde{\Omega}^*_{2k+2l}\delta\tilde{I}_{(2l+1)U} \\
&\qquad+\sum_{k=m+1}^{\infty}\sum_{l=0}^{\infty}\tilde{I}^*_{-2m+2k-1}\tilde{\Omega}_{2k+2l}\delta\tilde{I}^*_{(2l+1)L} \\
&\qquad+\sum_{k=m}^{\infty}\sum_{l=0}^{\infty}\tilde{I}^*_{-2m+2k+1}\tilde{\Omega}_{2k-2l}\delta\tilde{I}_{(2l+1)U} \\
&\qquad\left.+\sum_{k=0}^{\infty}\sum_{l=1}^{k}\tilde{I}_{2m+2k+1}\tilde{\Omega}^*_{2k-2l}\delta\tilde{I}^*_{(2l+1)L}\right) \\
&\quad-\frac{1}{4}\left(\sum_{k=0}^{m-1}\sum_{l=0}^{k}\tilde{I}_{2m-2k-1}\tilde{\Lambda}_{2k-2l+1}\delta\tilde{T}_{2lU}\right. \\
&\qquad+\sum_{k=-l}^{m-1}\sum_{l=1}^{\infty}\tilde{I}_{2m-2k-1}\tilde{\Lambda}_{2k+2l+1}\delta\tilde{T}^*_{2lL} \\
&\qquad+\sum_{k=\max(-l,-m)}^{\infty}\sum_{l=0}^{\infty}\tilde{I}_{2m+2k+1}\tilde{\Lambda}^*_{2k+2l+1}\delta\tilde{T}_{2lU} \\
&\qquad+\sum_{k=m}^{\infty}\sum_{l=1}^{\infty}\tilde{I}^*_{-2m+2k+1}\tilde{\Lambda}_{2k+2l+1}\delta\tilde{T}^*_{2lL} \\
&\qquad+\sum_{k=m}^{\infty}\sum_{l=0}^{k}\tilde{I}^*_{-2m+2k+1}\tilde{\Lambda}_{2k-2l+1}\delta\tilde{T}_{2lU} \\
&\qquad\left.+\sum_{k=0}^{\infty}\sum_{l=1}^{k}\tilde{I}_{2m+2k+1}\tilde{\Lambda}^*_{2k-2l+1}\delta\tilde{T}^*_{2lL}\right)=\frac{A}{2}\delta_{m0}.
\end{aligned}
\tag{67}
$$

The harmonic balance equation for the power at the lower sideband of the mth $(m \geq 1)$ harmonic, which has the frequency $2m\omega_0 - \omega$, is

$$
\begin{aligned}
&j(2m\omega_0-\omega)\gamma\left(\delta\tilde{T}_{2mL}+\delta_{m0}\delta\tilde{T}^*_{0U}\right) \\
&\quad+\frac{1}{2}\left(\sum_{l=1}^{m}\tilde{G}_{2m-2l}\delta\tilde{T}_{2lL}+\delta_{m0}G_0\delta\tilde{T}^*_{0U}+\sum_{l=0}^{\infty}\tilde{G}_{2m+2l}\delta\tilde{T}^*_{2lU}\right. \\
&\qquad\left.+\sum_{l=m}^{\infty}\tilde{G}^*_{-2m+2l}\delta\tilde{T}_{2lL}\right)
\end{aligned}
$$

$$
\begin{aligned}
&-\frac{1}{2}\left(\sum_{l=1}^{m-1}\tilde{V}_{2m-2l-1}\delta\tilde{I}_{(2l+1)L}+\sum_{l=0}^{\infty}\tilde{V}_{2m+2l+1}\delta\tilde{I}^{*}_{(2l+1)U}\right.\\
&\qquad\left.+\sum_{l=m}^{\infty}\tilde{V}^{*}_{-2m+2l+1}\delta\tilde{I}_{(2l+1)L}\right)\\
&-\frac{1}{4}\left(\sum_{k=0}^{m-1}\sum_{l=1}^{k}\tilde{I}_{2m-2k-1}\tilde{\Omega}_{2k-2l}\delta\tilde{I}_{(2l+1)L}\right.\\
&\qquad+\sum_{k=0}^{m}\sum_{l=1}^{\infty}\tilde{I}_{2m-2k+1}\tilde{\Omega}_{2k+2l}\delta\tilde{I}^{*}_{(2l+1)U}\\
&\qquad+\sum_{k=-l}^{-m}\sum_{l=1}^{\infty}\tilde{I}^{*}_{-2m-2k+1}\tilde{\Omega}^{*}_{2k+2l}\delta\tilde{I}_{(2l+1)L}\\
&\qquad+\sum_{k=\max(-l,1-m)}^{\infty}\sum_{l=1}^{\infty}\tilde{I}_{2m+2k-1}\tilde{\Omega}^{*}_{2k+2l}\delta\tilde{I}_{(2l+1)L}\\
&\qquad+\sum_{k=m+1}^{\infty}\sum_{l=0}^{\infty}\tilde{I}^{*}_{-2m+2k-1}\tilde{\Omega}_{2k+2l}\delta\tilde{I}^{*}_{(2l+1)U}\\
&\qquad+\sum_{k=m}^{\infty}\sum_{l=1}^{\infty}\tilde{I}^{*}_{-2m+2k+1}\tilde{\Omega}_{2k-2l}\delta\tilde{I}_{(2l+1)L}\\
&\qquad\left.+\sum_{k=0}^{\infty}\sum_{l=0}^{k}\tilde{I}_{2m+2k+1}\tilde{\Omega}^{*}_{2k-2l}\delta\tilde{I}^{*}_{(2l+1)U}\right)\\
&-\frac{1}{4}\left(\sum_{k=1}^{m-1}\sum_{l=1}^{k}\tilde{I}_{2m-2k-1}\tilde{\Lambda}_{2k-2l+1}\delta\tilde{T}_{2lL}\right.\\
&\qquad+\sum_{k=-l}^{m-1}\sum_{l=0}^{\infty}\tilde{I}_{2m-2k-1}\tilde{\Lambda}_{2k+2l+1}\delta\tilde{T}^{*}_{2lU}\\
&\qquad+\sum_{k=\max(-l,-m)}^{\infty}\sum_{l=1}^{\infty}\tilde{I}_{2m+2k+1}\tilde{\Lambda}^{*}_{2k+2l+1}\delta\tilde{T}_{2lL}\\
&\qquad+\sum_{k=m}^{\infty}\sum_{l=0}^{\infty}\tilde{I}^{*}_{-2m+2k+1}\tilde{\Lambda}_{2k+2l+1}\delta\tilde{T}^{*}_{2lU}\\
&\qquad+\sum_{k=m}^{\infty}\sum_{l=1}^{k}\tilde{I}^{*}_{-2m+2k+1}\tilde{\Lambda}_{2k-2l+1}\delta\tilde{T}_{2lL}\\
&\qquad\left.+\sum_{k=0}^{\infty}\sum_{l=0}^{k}\tilde{I}_{2m+2k+1}\tilde{\Lambda}^{*}_{2k-2l+1}\delta\tilde{T}^{*}_{2lU}\right)=\frac{A}{2}\delta_{m0}. \qquad (68)
\end{aligned}
$$

In (67) and (68), the complex amplitudes of the PSS current and voltage were defined in (26) and (27), and $\tilde{\Omega}$ and $\tilde{\Lambda}$ were defined in (43) and (44). They should be considered known parameters in (67) and (68) that were obtained from PSS analysis.

The PSS heat conductance G and its complex representation $\tilde{G}$, which have only even harmonic terms, are defined according to

$$\tilde{G}=\sum_{m=0}^{\infty}\tilde{G}_{2m}e^{j2\omega_0 t} \qquad (69)$$

$$G=\mathrm{Re}\tilde{G}=nKT_{pss}^{n-1} \qquad (70)$$

where the dc term $G_0=nKT_0^{n-1}$. As seen in Fig. 4(b), the dc component of T_{pss} is much larger than higher harmonic components. Consequently, G_0 is also much greater than higher harmonic terms.

The harmonic balance equation for the voltage at the upper and lower sidebands of the mth $(m\geq 0)$ harmonic, which has the frequency $(2m+1)\omega_0\pm\omega$, is

$$
\begin{aligned}
&\tilde{Z}_{RLC}\left((2m+1)\omega_0+\omega\right)\delta\tilde{I}_{(2m+1)U}\\
&+\frac{1}{2}\left(\sum_{l=0}^{m}\tilde{\Omega}_{2m-2l}\delta\tilde{I}_{(2l+1)U}\right.\\
&\qquad\left.+\sum_{l=0}^{\infty}\tilde{\Omega}_{2m+2l+2}\delta\tilde{I}^{*}_{(2l+1)L}+\sum_{l=m}^{\infty}\tilde{\Omega}^{*}_{-2m+2l}\delta\tilde{I}_{(2l+1)U}\right)\\
&\quad+\frac{1}{2}\left(\sum_{l=0}^{m}\tilde{\Lambda}_{2m-2l+1}\delta\tilde{T}_{2lU}+\sum_{l=1}^{\infty}\tilde{\Lambda}_{2m+2l+1}\delta\tilde{T}^{*}_{2lL}\right.\\
&\qquad\left.+\sum_{l=m+1}^{\infty}\tilde{\Lambda}^{*}_{-2m+2l-1}\delta\tilde{T}_{2lU}\right)=0 \qquad (71)
\end{aligned}
$$

$$
\begin{aligned}
&\tilde{Z}_{RLC}\left((2m+1)\omega_0-\omega\right)\delta\tilde{I}_{(2m+1)L}\\
&+\frac{1}{2}\left(\sum_{l=0}^{m}\tilde{\Omega}_{2m-2l}\delta\tilde{I}_{(2l+1)L}\right.\\
&\qquad\left.+\sum_{l=0}^{\infty}\tilde{\Omega}_{2m+2l+2}\delta\tilde{I}^{*}_{(2l+1)U}+\sum_{l=m}^{\infty}\tilde{\Omega}^{*}_{-2m+2l}\delta\tilde{I}_{(2l+1)L}\right)\\
&\quad+\frac{1}{2}\left(\sum_{l=1}^{m}\tilde{\Lambda}_{2m-2l+1}\delta\tilde{T}_{2lL}+\sum_{l=0}^{\infty}\tilde{\Lambda}_{2m+2l+1}\delta\tilde{T}^{*}_{2lU}\right.\\
&\qquad\left.+\sum_{l=m+1}^{\infty}\tilde{\Lambda}^{*}_{-2m+2l-1}\delta\tilde{T}_{2lL}\right)=0 \qquad (72)
\end{aligned}
$$

where Z_{RLC} was defined in (32).

Assuming terms in the PSS and PAC response, current, voltage, and temperature quickly decrease with harmonic m, i.e., $I_{2m+1}\gg I_{2(m+1)+1}$, $V_{2m+1}\gg V_{2(m+1)+1}$, $T_{2m}\gg T_{2(m+1)}$, $\delta I_{(2m+1)U}\gg\delta I_{(2(m+1)+1)U}$, $\delta I_{(2m+1)L}\gg\delta I_{(2(m+1)+1)L}$, $\delta T_{2mU}\gg\delta T_{(2(m+1))U}$, and $\delta T_{2mL}\gg\delta T_{(2(m+1))L}$, (67), (68), (71), and (72) can be approximately solved by working from lower to higher harmonics. Specifically, when $m=0$, by keeping only the largest terms and dropping terms at higher harmonics than $\delta\tilde{T}_{0U}$, $\delta\tilde{I}_{1U}$, and $\delta\tilde{I}_{1L}$, we obtain

(58)–(60) that can be used to solve for $\delta\tilde{T}_{0U}$, $\delta\tilde{I}_{1U}$, and $\delta\tilde{I}_{1L}$. Likewise, for $m = 1$, we have the following equations:

$$\left[G_0+j(2\omega_0+\omega)\gamma-\frac{1}{4}\left(\tilde{I}_1^*\tilde{\Lambda}_1+\tilde{I}_1\tilde{\Lambda}_1^*\right)\right]\delta\tilde{T}_{2U} -\frac{1}{2}\left(\tilde{V}_1^*+\Omega_0\tilde{I}_1^*\right)\delta\tilde{I}_{3U}=\frac{1}{2}(\tilde{V}_1+\Omega_0\tilde{I}_1)\delta\tilde{I}_{1U}+\frac{1}{4}\tilde{I}_1\tilde{\Lambda}_1\delta\tilde{T}_{0U} \tag{73}$$

$$\left[G_0+j(2\omega_0-\omega)\gamma-\frac{1}{4}\left(\tilde{I}_1^*\tilde{\Lambda}_1+\tilde{I}_1\tilde{\Lambda}_1^*\right)\right]\delta\tilde{T}_{2L} -\frac{1}{2}\left(\tilde{V}_1^*+\Omega_0\tilde{I}_1^*\right)\delta\tilde{I}_{3L}=\frac{1}{2}(\tilde{V}_1+\Omega_0\tilde{I}_1)\delta\tilde{I}_{1L}+\frac{1}{4}\tilde{I}_1\tilde{\Lambda}_1\delta\tilde{T}_{0U}^* \tag{74}$$

$$\left[\tilde{Z}_{RLC}(3\omega_0+\omega)+\Omega_0\right]\delta\tilde{I}_{3U}+\frac{1}{2}\tilde{\Lambda}_1\delta\tilde{T}_{2U} =-\frac{1}{2}\tilde{\Lambda}_3\delta\tilde{T}_{0U}-\frac{1}{2}\tilde{\Omega}_2\delta\tilde{I}_{1U} \tag{75}$$

$$\left[\tilde{Z}_{RLC}(3\omega_0-\omega)+\Omega_0\right]\delta\tilde{I}_{3L}+\frac{1}{2}\tilde{\Lambda}_1\delta\tilde{T}_{2L} =-\frac{1}{2}\tilde{\Lambda}_3\delta\tilde{T}_{0U}^*-\frac{1}{2}\tilde{\Omega}_2\delta\tilde{I}_{1L}. \tag{76}$$

In (73)–(76), $\delta\tilde{T}_{0U}$, $\delta\tilde{I}_{1U}$, and $\delta\tilde{I}_{1L}$ should be considered known parameters. Because we have obtained their values in the previous step, it is now possible to solve for $\delta\tilde{T}_{2U}$, $\delta\tilde{T}_{2L}$, $\delta\tilde{I}_{3U}$, and $\delta\tilde{I}_{3L}$ using (73)–(76). Comparing (73) and (74) to (58), we see that the higher harmonic thermal equations have effective input power due to lower harmonic signals. This, again, is the frequency translation behavior of ac-biased nonlinear circuits at work, since power is transferred from the fundamental frequency to higher harmonics [20]. Likewise, (75) and (76) suggest that higher harmonic electrical equations have effective bias voltages due to signals at lower harmonics.

This method of solving for higher harmonic terms based on lower harmonic terms that have already been obtained can be generalized to arbitrary harmonic m. The equations for the mth $(m > 1)$ harmonic are

$$\begin{aligned}&\left[G_0+j(2m\omega_0+\omega)\gamma-\frac{1}{4}\left(\tilde{I}_1^*\tilde{\Lambda}_1+\tilde{I}_1\tilde{\Lambda}_1^*\right)\right]\delta\tilde{T}_{2mU} -\frac{1}{2}\left(\tilde{V}_1^*+\Omega_0\tilde{I}_1^*\right)\delta\tilde{I}_{(2m+1)U}\\ &=\frac{1}{2}\sum_{l=0}^{m-1}(\tilde{V}_{2m-2l-1}+\Omega_0\tilde{I}_{2m-2l-1})\delta\tilde{I}_{(2l+1)U} +\frac{1}{4}\sum_{k=l+1}^{m-1}\sum_{l=0}^{m-1}\tilde{\Omega}_{2k-2l}\tilde{I}_{2m-2k-1}\delta\tilde{I}_{(2l+1)U}\\ &\quad+\frac{1}{4}\sum_{k=0}^{m-1}\sum_{l=0}^{k}\tilde{I}_{2m-2k-1}\tilde{\Lambda}_{2k-2l+1}\delta\tilde{T}_{2lU}\end{aligned} \tag{77}$$

$$\begin{aligned}&\left[G_0+j(2m\omega_0-\omega)\gamma-\frac{1}{4}\left(\tilde{I}_1^*\tilde{\Lambda}_1+\tilde{I}_1\tilde{\Lambda}_1^*\right)\right]\delta\tilde{T}_{2mL} -\frac{1}{2}\left(\tilde{V}_1^*+\Omega_0\tilde{I}_1^*\right)\delta\tilde{I}_{(2m+1)L}\\ &=\frac{1}{2}\sum_{l=1}^{m-1}(\tilde{V}_{2m-2l-1}+\Omega_0\tilde{I}_{2m-2l-1})\delta\tilde{I}_{(2l+1)L} +\frac{1}{4}\sum_{k=l+1}^{m-1}\sum_{l=1}^{m-1}\tilde{\Omega}_{2k-2l}\tilde{I}_{2m-2k-1}\delta\tilde{I}_{(2l+1)L}\\ &\quad+\frac{1}{4}\sum_{k=1}^{m-1}\sum_{l=1}^{k}\tilde{I}_{2m-2k-1}\tilde{\Lambda}_{2k-2l+1}\delta\tilde{T}_{2lL}\end{aligned} \tag{78}$$

$$\left[\tilde{Z}_{RLC}\left((2m+1)\omega_0+\omega\right)+\Omega_0\right]\delta\tilde{I}_{(2m+1)U}+\frac{1}{2}\tilde{\Lambda}_1\delta\tilde{T}_{2mU} =-\frac{1}{2}\sum_{l=0}^{m-1}\tilde{\Lambda}_{2m-2l+1}\delta\tilde{T}_{2lU}-\frac{1}{2}\sum_{l=0}^{m-1}\tilde{\Omega}_{2m-2l}\delta\tilde{I}_{(21+1)U} \tag{79}$$

$$\left[\tilde{Z}_{RLC}\left((2m+1)\omega_0-\omega\right)+\Omega_0\right]\delta\tilde{I}_{(2m+1)L}+\frac{1}{2}\tilde{\Lambda}_1\delta\tilde{T}_{2mL} =-\frac{1}{2}\sum_{l=1}^{m-1}\tilde{\Lambda}_{2m-2l+1}\delta\tilde{T}_{2lL}-\frac{1}{2}\sum_{l=1}^{m-1}\tilde{\Omega}_{2m-2l}\delta\tilde{I}_{(21+1)L}. \tag{80}$$

APPENDIX B
DEVICE MODEL AND SIMULATION FILES

All circuit simulation in this work is performed using SpectreRF, which is a proprietary circuit simulator developed by Cadence Design Systems, Inc. For detailed information about Spectre and the company, visit http://www.cadence.com. For the readers' benefit, we include the device model file and circuit simulation files. They can be freely used as long as this work and earlier work on this topic [10], [11] are properly acknowledged and cited.

A. TES Device Model for Spectre: We built a behavioral device model [11] for TES using the IV relation (16) and Verilog-A, which is an analog hardware description language (AHDL) supported by Spectre. An AHDL can model the electrical behavior of a device using mathematical and logic expressions, rather than modeling based on more elementary circuit elements (such as a resistor, an inductor, and a capacitor) and, thus, is a convenient and powerful tool to model devices with complicated and nonlinear behavior. The resulting device model can be understood by supporting circuit simulators and used in circuit simulation. For a detailed description of the TES behavioral modeling and circuit simulation, see [11].

The Verilog-A model for TES is shown in Listing 1. Lines starting with // are comments.

```
// VerilogA file for TES model

// necessary header files

`include "discipline.h"
`include "constants.h"

// Device module declaration
// with 4 terminals
module tes(P1, P2, Ttes, Tb);
// input-output ports: the two
// electrical connection ports
// and the TES temperature
inout P1,P2,Ttes;
// input port: the bath temperature
input Tb;

electrical P1,P2,Ttes,Tb;

// device parameters that can be specified
// when the device is used in a netlist
parameter real
// critical temperature
Tc=0.105,
Cr=1,
// normal resistance
Rn=1.6,
// 0-temperature critical current
Is0=35u,
// heat conduction coefficient
kg=16.54n,
// heat conduction exponent
n=5,
// heat capacity
Cap=3.3f;

// The crtitical current
real Is;

// analog behavioral modeling
analog begin

// dependence of critical
// current on temperature
// + sign at the beginning of
// a line means continuation
// of the last line
Is=(V(Ttes)>=Tc) ? 0 :(Is0
+ *pow((1-V(Ttes)/Tc),1.5));

// I-V characteristic of the TES
if (V(Ttes)<Tc) begin
if (I(P1,P2)>=Is)
V(P1,P2)<+(I(P1,P2)-Is)*Rn*Cr;
else if (I(P1,P2)<=-Is)
V(P1,P2)<+(I(P1,P2)+Is)*Rn*Cr;
else
V(P1,P2)<+0;
end
else
V(P1,P2)<+I(P1,P2)*Rn*Cr;

// thermal equation
I(Ttes,Tb)<+Cap*ddt(V(Ttes))+
-I(P1,P2)*V(P1,P2)
+ +kg*(pow(V(Ttes),n)-pow(V(Tb),n));
end
endmodule
```

Listing 1. Verilog-A model for TES.

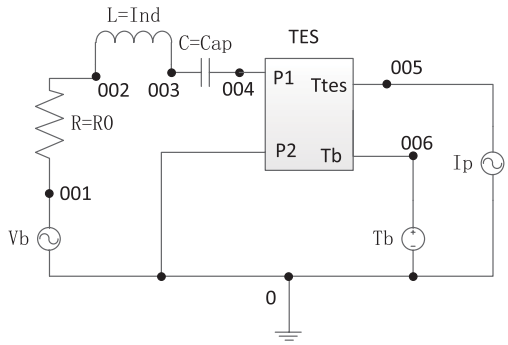

Fig. 12. Circuit diagram for the transient, PSS, and PAC simulation.

B. Simulation Files: The following are Spectre files for simulation results presented in this paper. They can be run by Spectre directly, provided that the device model file in Listing 1 is placed in the appropriate directory and can be found and loaded by Spectre. Although in our work, we do not write the simulation file and run Spectre manually. Instead, we take advantage of the integrated Cadence IC design environment to draw the circuit, generate the netlist, and run the simulation through a graphical user interface. How this is done is described in [10] and [11] as well as in the Cadence documentation in much greater detail. Such a workflow is recommended if the design suite is available, since it greatly improves design efficiency and reduces human error.

1) Transient Simulation: The diagram of the ac-biased TES circuit is shown in Fig. 12. The simulation file is in Listing 2. The TES device model, which is shown in Listing 1, is saved in a file named "tes.va" in the same directory with the simulation file. The result of the simulation is plotted in Figs. 4 and 5.

2) PSS Simulation: The diagram of the ac-biased TES circuit is shown in Fig. 12. The amplitude of the ac bias voltage, i.e., V_b, is the sweeping parameter for the simulation. The simulation file is in Listing 3. The TES device model, which is shown in Listing 1, is saved in a file named "tes.va" in the same directory with the simulation file. The simulation result is plotted in Fig. 6. Notice that, for the hysteresis plot in Fig. 6, two PSS simulations are run, in which V_b values are swept from low to high and from high to low, respectively. Moreover, to obtain the hysteresis, it is critical to set the initial condition T_i for the TES temperature T appropriately. When V_b is swept from low to high, T_i should be set to a value below the environment temperature T_b. When V_b is swept from high to low, T_i should be set to a value close to the critical temperature T_c. This is necessary because in the area with hysteresis, there are two possible PSS with the TES temperature close to T_b and T_c, respectively. Generally speaking, the simulator will settle in the state closer to the initial condition.

3) PAC Simulation: The diagram of the simulated circuit is shown in Fig. 12. A single-frequency input signal $A\cos(\omega t)$ is assumed, and its frequency is swept at different harmonic m values of carrier frequency ω_0. The simulation file is in Listing 4. The TES device model, which is shown in Listing 1, is saved in a file named "tes.va" in the same directory with the simulation file. The simulation result is plotted in Fig. 11.

```
// simulator name
simulator lang=spectre

// global ground net
global 0

// circuit parameter declaration:
parameters
// inductance

Ind=50n
// capacitance
Cap=100u
// AC bias voltage
Vb=500n
pi=3.141592653
// frequency of the bias voltage
freq0=1/(2*pi*sqrt(Ind*Cap))
// resistance
R0=17.5
// input signal power
Ip=3f
// bath temperature
Tb=55m

// circuit netlist
// bias voltage
Vb (net001 0) vsource type=sine ampl=Vb \
freq=freq0

R0 (net001 net002) resistor r=R0
L1 (net002 net003) inductor l=Ind
C1 (net003 net004) capacitor c=Cap

// The TES. Device parameters are the
// default values set in the model file.
// They should be specified if this is
// not the case.
TES (net004 0 net005 net006) tes

// input signal power: since mag=0 the
// signal power in transient analysis is
// 0. pacmag=Ip means the signal power is
// set to Ip only in PAC analysis.
Ip (0 net005) isource dc=0 mag=0 type=sine
pacmag=Ip sinedc=0

// bath temperature
Vt (net005 0) vsource dc=55m type=dc

// simulation settings and options
simulatorOptions options reltol=1e-4
vabstol=1e-6 iabstol=1e-12
gmin=1e-15 rforce=1
digits=5 cols=80 pivrel=1e-3
ckptclock=1800

// transient simulation
tran tran stop=11m outputstart=10m
step=10n maxstep=10n

// include the TES device model
ahdl_include "./tes.va"
```

Listing 2. Spectre file for transient analysis of the ac-biased TES circuit in Fig. 12 without an input signal ($I_p = 0$ in Fig. 12).

```
// simulator name
simulator lang=spectre

// global ground node
global 0

// circuit parameters
parameters Ind=50n Cap=100u
Vb=500n pi=3.141592653
freq0=1/(2*pi*sqrt(Ind*Cap)) R0=17.5 Ip=3f
Tb=55m

// circuit netlist
// the bias voltage
Vb (net001 0) vsource type=sine ampl=Vb
freq=freq0

R0 (net001 net002) resistor r=R0
L1 (net002 net003) inductor l=Ind
C1 (net003 net004) capacitor c=Cap

// The TES. Device parameters are the
// default values set in the model file.
// They should be specified if this is
// not the case.
TES (net004 0 net005 net006) tes

// input signal power: since mag=0 the
// signal power in pss analysis is
// 0. pacmag=Ip means the signal power is
// set to Ip only in PAC analysis.
Ip (0 net005) isource dc=0 mag=0 type=sine
pacmag=Ip sinedc=0

// the bath temperature
Vt (net006 0) vsource dc=55m type=dc

// the initial condition for the
// TES temperature
ic net005=0.05

// simulation options
simulatorOptions options reltol=1e-4
vabstol=1e-6 iabstol=1e-12
gmin=1e-15 rforce=1
digits=5 cols=80 pivrel=1e-3
ckptclock=1800

// PSS simulation. Vb is swept.
sweeppss sweep param=Vb start=0 stop=0.9u
step=0.003u {
pss pss fund=71.1763K harms=20
errpreset=conservative tstab=10u
annotate=status
}

// include the TES device model
ahdl_include "./tes.va"
```

Listing 3. Spectre file for PSS analysis of the ac-biased TES circuit in Fig. 12.

ACKNOWLEDGMENT

The authors would like to thank the Center for Information Science at the University of Science and Technology of China for providing access to the EDA software used in this research.

```
// simulator name
simulator lang=spectre

// global ground net
global 0

// circuit parameters:
parameters Ind=50n Cap=100u
Vb=500n pi=3.141592653
freq0=1/(2*pi*sqrt(Ind*Cap)) R0=17.5 Ip=3f
Tb=55m

// circuit netlist
// the bias voltage
Vb (net001 0) vsource type=sine ampl=Vb
freq=freq0

R0 (net001 net002) resistor r=R0
L1 (net002 net003) inductor l=Ind
C1 (net003 net004) capacitor c=Cap

// The TES. Device parameters are the
// default values set in the model file.
// They should be specified if this is
// not the case.
TES (net004 0 net005 net006) tes

// the input signal power is 0 in PSS

// and Ip in PAC
Ip (0 net005) isource dc=0 mag=0 type=sine
pacmag=Ip sinedc=0

// the bath temperature
Vt (net006 0) vsource dc=55m type=dc

// initial condition for
// the TES temperature
ic net005=0.05

// simulation Options
simulatorOptions options reltol=1e-4
vabstol=1e-6 iabstol=1e-12
gmin=1e-15 rforce=1
digits=5 cols=80 pivrel=1e-3
ckptclock=1800

// PAC simulation - A PSS simulation
// must be performed first
pss pss fund=71.1763K harms=20
errpreset=conservative tstab=10u
annotate=status
pac pac start=100 stop=100k maxsideband=20
annotate=status

// include the TES device model
ahdl_include "./tes.va"
```

Listing 4. Spectre file for PAC analysis of the ac-biased TES circuit in Fig. 12.

REFERENCES

[1] P. A. R. Ade *et al.*, "Detection of B-mode polarization at degree angular scales by BICEP2," *Phys. Rev. Lett.*, vol. 112, no. 24, Jun. 2014, Art. ID. 241101.

[2] P. D. Mauskopf *et al.*, "A TES focal plane for SPICA-SAFARI," in *Proc. 21st Int. Symp. Space THz Technol.*, 2010, pp. 246–255.

[3] L. Gottardi *et al.*, "Development of TES-based detectors array for the X-ray integral field unit (X-IFU) on the future X-ray observatory ATHENA," *Proc. SPIE*, vol. 9144, 2014, pp. 1–7.

[4] J. van der Kuur *et al.*, "Small-signal behavior of a TES under AC bias," *IEEE Trans. Appl. Supercond.*, vol. 21, no. 3, pp. 281–284, Jun. 2011.

[5] M. A. Lindeman, P. Khosropanah, and R. A. Hijmering, "Model of superconducting alternating current bolometers," *J. Appl. Phys.*, vol. 113, no. 7, Feb. 2013, Art. ID. 074502.

[6] K. S. Kundert, "Introduction to RF simulation and its application," *IEEE J. Solid-State Circuits*, vol. 34, no. 9, pp. 1298–1319, Sep. 1999.

[7] M. A. Lindeman, "Microcalorimetry and the transition-edge sensor," Ph.D. dissertation, Univ. California, Davis, CA, USA, 2000.

[8] M. A. Lindeman *et al.*, "Impedance measurements and modeling of a transition-edge-sensor calorimeter," *Rev. Sci. Instrum.*, vol. 75, no. 5, p. 1283, 2004.

[9] K. D. Irwin and G. C. Hilton, "Transition-edge sensors," *Topics Appl. Phys.*, vol. 99, pp. 63–150, 2005.

[10] T.-S. Wang *et al.*, "Device modeling of superconductor transition-edge sensors," *IEEE Trans. Appl. Supercond.*, vol. 22, no. 4, Aug. 2012, pp. 1298–1319, Art. ID. 2100212.

[11] T.-S. Wang *et al.*, "Simplified two-fluid current–voltage relation for superconductor transition-edge sensors," *Nucl. Instrum. Methods Phys. Res. A, Accel. Spectrom. Detect. Assoc. Equip.*, vol. 729, pp. 474–483, Nov. 2013.

[12] A. V. Oppenheim and A. S. Willsky, *Signals and Systems*, 2nd ed. Englewood Cliffs, NJ, USA: Prentice-Hall, 1996.

[13] M. Galeazzi and D. McCammon, "Microcalorimeter and bolometer model," *J. Appl. Phys.*, vol. 93, no. 8, pp. 4856–4869, Apr. 2003.

[14] K. D. Irwin, G. C. Hilton, D. A. Wollman, and J. M. Martinis, "Thermal-response time of superconducting transition-edge microcalorimeters," *J. Appl. Phys.*, vol. 83, no. 8, pp. 3978–3985, 1998.

[15] D. A. Bennett, D. R. Schmidt, D. S. Swetz, and J. N. Ullom, "Phase-slip lines as a resistance mechanism in transition-edge sensors," *Appl. Phys. Lett.*, vol. 104, no. 4, 2014, Art. ID. 042602.

[16] D. A. Bennett, D. S. Swetz, D. R. Schmidt, and J. N. Ullom, "Resistance in transition-edge sensors: A comparison of the resistively shunted junction and two-fluid models," *Phys. Rev. B, Condens. Matter*, vol. 87, no. 2, Jan. 2013, Art. ID. 020508.

[17] L. Gottardi1 *et al.*, "Josephson effects in an alternating current biased transition edge sensor," *Appl. Phys. Lett.*, vol. 105, no. 16, 2014, Art. ID. 162605.

[18] E. Taralli, C. Portesi, R. Rocci, M. Rajteri, and E. Monticone, "Investigation of Ti/Pd bilayer for single photon detection," *IEEE Trans. Appl. Supercond.*, vol. 19, no. 3, pp. 493–495, Jun. 2009.

[19] N. H. R. Baars, J. Van der Kuur, M. P. Lubbers, and P. A. J. de Korte, "First results of a TES microcalorimeter AC-biased at 500 kHz," *Nucl. Instrum. Methods Phys. Res. A, Accel. Spectrom. Detect. Assoc. Equip.*, vol. 520, pp. 574–577, Mar. 2004.

[20] B. Razavi, *RF Microelectronics*. Englewood Cliffs, NJ, USA: Prentice-Hall, 2012.

Authors' biographies not available at the time of publication.